Journal of Membrane Science 497 (2016) 239–247

Contents lists available at ScienceDirect

Journal of Membrane Science

journal homepage: www.elsevier.com/locate/memsci

Exploring the potential of commercial polyethylene membranes for desalination by membrane distillation

Jian Zuo [a], Sina Bonyadi [b], Tai-Shung Chung [a,c,*]

[a] Department of Chemical & Biomolecular Engineering, National University of Singapore, 4 Engineering Drive 4, 117585, Singapore
[b] Entegris, Inc., 129 Concord Road, Billerica, MA 01821, United States
[c] Water Desalination & Reuse (WDR) Center, King Abdullah University of Science and Technology, Thuwal 23955-6900, Saudi Arabia

ARTICLE INFO

Article history:
Received 27 May 2015
Received in revised form
14 September 2015
Accepted 15 September 2015
Available online 25 September 2015

Keywords:
Polyethylene (PE)
Membrane distillation
Sea water desalination

ABSTRACT

The potential of utilizing polyethylene (PE) membranes in membrane distillation (MD) for sea water desalination has been explored in this study. The advantages of using PE membranes are (1) their intrinsic hydrophobicity with low surface energy of 28–33 $\times 10^{-3}$ N/m, (2) good chemical stability and low thermal conductivity and (3) their commercial availability that may expedite the MD commercialization process. Several commercial PE membranes with different physicochemical properties are employed to study the capability and feasibility of PE membrane application in an MD process. The effect of membrane pore size, porosity, thickness and wetting resistance on MD performance and energy efficiency have been investigated. The PE membranes demonstrate impressive separation performance with permeation fluxes reaching 123.0 L/m^2 h for a 3.5 wt% sodium chloride (NaCl) feed solution at 80 °C. This superior performance surpasses most of the prior commercial and lab-made flat sheet and hollow fiber membranes. A long term MD testing of 100 h is also performed to evaluate the durability of PE membranes, and a relatively stable performance is observed during the entire experiment. This long term stability signifies the suitability of PE membranes for MD applications.

1. Introduction

Along with rapid population growth, the water scarcity issue has become one of the most imperative problems globally. Today, about 1 billion people are suffering from the deficiency of drinkable water [1]. The water shortage would become more severe in the future due to acceleration of urbanization and industrialization [2,3]. To alleviate the water crisis, sea water desalination and waste water reclamation have received great attention for fresh water production. Conventional desalination methods, such as multi-stage flash distillation (MSF), multiple-effect distillation (MED) or sea water reverse osmosis (SWRO) have been utilized commercially for fresh water production. Nevertheless, researchers are always trying to further improve the desalination technologies. Among many attempts, membrane distillation (MD) stands out as a potentially promising alternative owing to: (1) mild operation conditions as compared to traditional methods, (2) 100% theoretical rejection to salts, (3) small foot print (4) less sensitive to feed salinity for desalination and (5) the ability to couple with low grade heat such as incinerator heat or renewable energy sources such as solar and geothermal energy [4–8].

MD is a thermally driven process based on vapor–liquid equilibrium. The separation process involves three steps: the evaporation of water from the hot feed solution, the migration of water vapor across the microporous membrane and the condensation of permeate at the other side [8–10]. To create the chemical potential difference across the MD membrane, four types of configurations for the permeate side have been designed. In direct contact membrane distillation (DCMD), cold water is employed to receive the permeated vapor. In vacuum membrane distillation (VMD), the water vapor is drawn by a vacuum pump. The other two configurations utilize either sweep gas to carry the permeate or cold surface to condensate the water vapor, which are referred to as sweep gas membrane distillation (SGMD) and air gas membrane distillation (AGMD). Among them, DCMD is the most widely used mode in desalination because of its simplicity and ease of operation, and thus is used in this study [11,12].

Membrane is one of the most important factors for a successful MD process. The MD membrane provides an interface for retaining the liquid water feed and salts, while allowing the water vapor to pass through it. There is always a risk of membrane wetting by water, which may lead to the loss of membrane selectivity when the membrane pores are entirely wetted [13]. Therefore,

* Corresponding author at: Department of Chemical & Biomolecular Engineering, National University of Singapore, 4 Engineering Drive 4, 117585, Singapore. Fax: +65 6779 1936.
E-mail address: chencts@nus.edu.sg (T.-S. Chung).

http://dx.doi.org/10.1016/j.memsci.2015.09.038
0376-7388/

membrane hydrophobicity becomes an essential property, which must be good enough to prevent the feed liquid from penetrating into membrane pores [14–16]. This hydrophobic characteristic has limited polymeric materials that could be used for MD. Some common hydrophobic materials, such as polyvinylidene fluoride (PVDF), polytetrafluoro-ethylene (PTFE), polypropylene (PP) have been extensively studied for the fabrication of MD membranes [17–19]. Some excellent MD membranes have been reported from these materials. For instance, lotus-root-like multi-bore hollow fiber membranes with good water production rate and salt rejection, and excellent tensile properties have been designed from PVDF [17]. PTFE membranes with a large porosity of 70% with controlled pore size and pore size distribution have been developed using melt extrusion followed by stretch operations [18].

In spite of various membranes studied in the literature, the commercialization of MD processes is still restricted by the lack of commercially available high performance membranes [19,20]. Other than the development of lab scale membranes, the investigation of potential commercial membranes may offer another perspective [21,22]. Therefore, in this study, several commercial polyethylene (PE) membranes have been employed to explore their prospect in DCMD for clean water production. PE is hydrophobic in nature and meets the essential requirement of MD membranes. It has a low surface energy of $28–33 \times 10^{-3}$ N/m, which is similar to that of PVDF and PP materials [20]. Moreover, PE also has good chemical stability and low thermal conductivity. However, the report of using PE membranes for MD is rather limited [23]. Li et al. have used microporous PP and PE hollow fiber membranes made from melt-extrusion/cold-stretching methods in DCMD for desalination. It was found that PE membranes permeated more distillate water than PP membranes [23]. Although there is limited report on application of stretched PE membranes in an MD process, there appears to be no report on the application of PE membranes made by thermally induced phase separation (TIPS). Therefore, the possibility of applying PE membranes in MD and especially those made by TIPS process should not be overlooked. The use of commercially available PE membranes may also expedite the commercialization process of MD technology.

Hence, the objectives of this work are to (1) evaluate the capability of several commercially available TIPS-made PE membranes in DCMD for seawater desalination; (2) investigate the effects of membrane physicochemical properties, such as morphology, pore size, hydrophobicity on flux, retention and separation effectiveness; and (3) analyze the energy efficiency of these membranes. In addition, the thermal stability of PE membranes is studied under high operation temperatures. Lastly, a long term MD test of 100 h is also performed to evaluate the durability of PE membranes. This study may provide useful insights on PE membranes and open up new opportunities for them to be used in MD for seawater desalination.

2. Experimental

2.1. Materials

Polyethylene (PE) flat sheet membranes with different pore sizes (M1, M2, and M3) and thicknesses (M4) were provided by Entegris Inc. The commercial names of the four membranes are TPZP, TPVP, TPGP and UPZP, respectively. The membranes were cut into pieces for characterizations and DCMD tests without any pretreatment. Sodium chloride (NaCl) was purchased from Merck and used to prepare the model sea water. The deionized water used in DCMD experiments was produced by a Milli-Q unit from MilliPore with the resistivity of 18 MΩ cm.

2.2. Membrane characterizations

Field emission scanning electron microscopy (FESEM JEOL JSM-6700LV) was used to observe membrane morphologies. The FESEM samples were prepared by fracturing the PE membranes in liquid nitrogen and coated with platinum using a JEOL JFC-1200 ion sputtering device.

The average pore sizes of the PE membranes were measured by a CFP-1500 AE capillary flow porometer (PMI, Vista, CA). A PMI Galwick solution with a surface tension of 15.9 dynes/cm was used to prepare the membrane samples. A piece of membrane was immersed in the Galwick solution for 1 day to assure total wetting before loading it into the porometer.

The membrane porosity ε was calculated by Eq. (1):

$$\varepsilon = \left(1 - \frac{m_{\text{memb}}/V_{\text{memb}}}{\rho_{\text{mater}}}\right) \times 100\% \tag{1}$$

where m_{memb} and V_{memb} are the weight and volume of a piece of membrane, while ρ_{mater} is the density of the membrane material. m_{memb} Was measured by an accurate balance (A&D, GR-200). V_{memb} Was obtained from the dimension of the membrane sample. ρ_{mater} was measured with a density kit and Mettler Toledo balance by applying the Archimedean principle. Firstly, a piece of the dry membrane was weighed in air. Then, it was weighed again while immersion in an analytic grade hexane solution. The density of the membrane material is calculated according to the following equation:

$$\rho_{\text{mater}} = \left(\frac{w_{\text{air}}}{w_{\text{air}} - w_{\text{hexane}}}\right) \times \rho_{\text{hexane}} \tag{2}$$

where w_{air} and w_{hexane} are the membrane weights in air and hexane, respectively, and ρ_{hexane} is the density of hexane. The density value for the current PE material was obtained to be 0.99 g/cm^3.

To understand the roughness and topology of the membrane surfaces with different pore sizes, a Nanoscope IIIa atomic force microscope (AFM) from Digital Instruments Inc was used. The measurements were carried out on 5×5 μm^2 areas. For each membrane, several locations were scanned, and the average value was reported. The root mean square roughness (R_{ms}), average roughness (R_{a}) and maximum roughness (R_{max}) were calculated based on AFM measurements.

The water contact angle of PE membranes were measured by a Rame-Hart Contact Angle Goniometer (model 100-22). Deionized water was dropped onto the membrane surface by a Gilmont micro-syringe. The contact angle was measured once the droplet was formed on the surface. At least 10 droplets were introduced and the average contact angle was reported to ensure the accuracy.

To study wetting resistance, the liquid entry pressures (LEP) of PE membranes were determined by a lab-made setup [11]. As shown in Fig. 1, a 200 ml stainless steel tube was used as the reservoir for salt water (NaCl 3.5 wt%). A pressure gauge was connected to the top of tube. Before the measurement, the membrane module was assembled in a way that the outlet of the feed side was sealed. During testing, the inlet of the feed side was connected to the reservoir tube, and the whole module was then immersed in a deionized water bath. The hydraulic pressure was introduced by compressed nitrogen, and increased with a step of 0.05 bar at an interval of 5 min. The conductivity of the water bath was constantly monitored by a conductivity meter Lab 960 m ($0–500$ ms cm^{-1}, $\pm$ 0.1 μs cm^{-1} for the measuring range of 0–200 μs cm^{-1}, SCHOOT instrument). Eventually, the pressure at which the water conductivity increased sharply was determined as the LEP of the membrane.

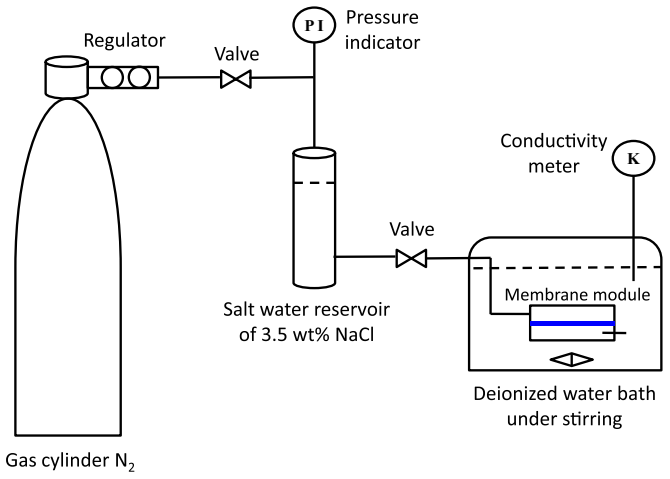

Fig. 1. Schematic drawing of lab-made setup for LEP measurement.

To analyze the thermal stability of PE membranes, the melting point temperature (T_m) of the membranes were measured by a TA Instrument 2920 modulated differential scanning calorimeter (DSC). A heating rate of 3 °C/min with an oscillation amplitude of ± 0.65 °C was used and the thermal response curve was recorded.

2.3. DCMD desalination experiments

DCMD desalination experiments were carried out to evaluate the performance of PE membranes. Fig. 2 depicts the schematic drawing of a laboratory-scale setup [24,25]. Before running the experiment, a PE membrane sample was mounted onto the testing module, with an effective membrane area of 10 cm^2. The dimension of feed and permeate flow channels was the same, which was rectangular and had a cross-section of 1×1 cm^2 and a length of 10 cm. A 5-l 3.5 wt% NaCl solution was used as the feed solution, while deionized water was employed as the permeate stream. The feed temperature was controlled by a heater at four designated values, namely, 50, 60 70 and 80 °C. It was circulated to the feed side of the membrane by a centrifugal pump, and the flow rate was regulated at three different values of 30, 60 and 90 L/h. On the other hand, the permeate stream was stored in a 1-l tank, and the temperature was reduced by a cooler to 17 °C. It was circulated by a rotary pump along the permeate side of the membrane with a flow rate of 24 L/h. To monitor the temperature change during the testing, the outlet temperatures of the feed and permeate streams were also recorded by digital thermocouples. For each condition, the membrane module was tested for 30 min to ensure accuracy, and one membrane module was tested for all four feed temperatures. The permeation flux was calculated according to Eq. (3):

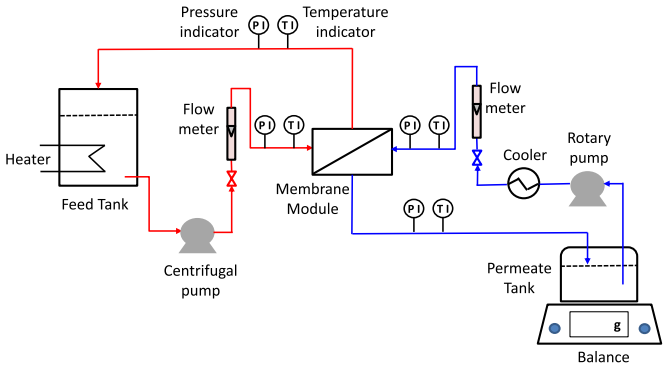

Fig. 2. Schematic drawing of DCMD setup.

$$N_w = \frac{m}{A \times t} \tag{3}$$

where N_w is the permeation flux, m is the mass of the permeate sample collected over time t, A is the effective membrane area. The ionic conductivity of the permeate stream was monitored by a conductivity meter Lab 960 m (0–500 ms cm^{-1}, ± 0.1 μs cm^{-1} for the measuring range of 0–200 μs cm^{-1}, SCHOOT instrument) during the DCMD tests, and there was no salt leakage observed. It may be worried that under current operation conditions, the collected permeate sample may not be enough as compared to the permeate tank to detect any salt leakage. A control DCMD experiment was carried out. The permeate steam volume was reduced to 400 ml, and the sampling time was increased to 2 h. The M1 membrane was used and the feed temperature was set at 80 °C. This control condition was chosen because of its higher wetting possibility. A permeate sample of 167 ml was collected, which was good enough to detect any wetting phenomena. The permeate stream conductivity was not changed during the entire experiment, which indicated no salt leakage. This double confirmed that the PE membranes were not wetted during the DCMD experiments.

Some of the MD experiments were repeated to ensure the reproducibility of permeation performance of the PE membranes. Errors in terms of permeate fluxes were all within 10%. This signifies the consistence of the PE membranes.

For the long-term DCMD experiment, similar operation conditions were used as in short-term experiments. The feed solution and permeate stream temperatures were controlled at 60 °C and 17 °C, respectively. The feed solution flow rate was fixed at 90 L/h. The M1 membrane was used in this test, and the experiment was run for 100 h. Due to safety reason, the experiment was carried out during the day time. At night, the temperature and circulation for both the feed and permeation sides were stopped. However, the membrane was not removed from the system during night. The counting of 100 h was based on the real running time during the day. To maintain the feed solution salinity, the produced distillate was recycled back to the feed tank. The separation factor (β) was calculated according to Eq. (4):

$$\beta = \left(1 - \frac{c_p}{c_f}\right) \times 100\% \tag{4}$$

where c_p and c_f are the NaCl concentrations in permeate and feed solutions, respectively.

3. Results and discussion

3.1. Characterizations of PE flat sheet membranes

3.1.1. Membrane morphology

Fig. 3(a–c) displays the surface morphology of PE membranes, M1, M2 and M3. Visible pores are observed on the surfaces under a magnification of 2K, which indicates microporous nature of the membranes. The observed surface pore sizes have an increasing trend from M1 to M3. The average pore sizes of the three membranes are measured by an in-house PMI porometer. As listed in Table 1, the pore size increases from 0.06 to 0.21 μm for M1 to M3, which is consistent with FESEM observation. Typically, pore sizes from 0.1 to 0.6 μm are recommended for the DCMD process [26,27]. These values ensure a high permeation flux while preventing membrane wetting under different operation conditions. Therefore, the PE membranes in this study have suitable pore sizes and meet the pore size requirement for DCMD. It may be noted that the measured pore sizes differ slightly from those provided by the company probably due to different measurement techniques.

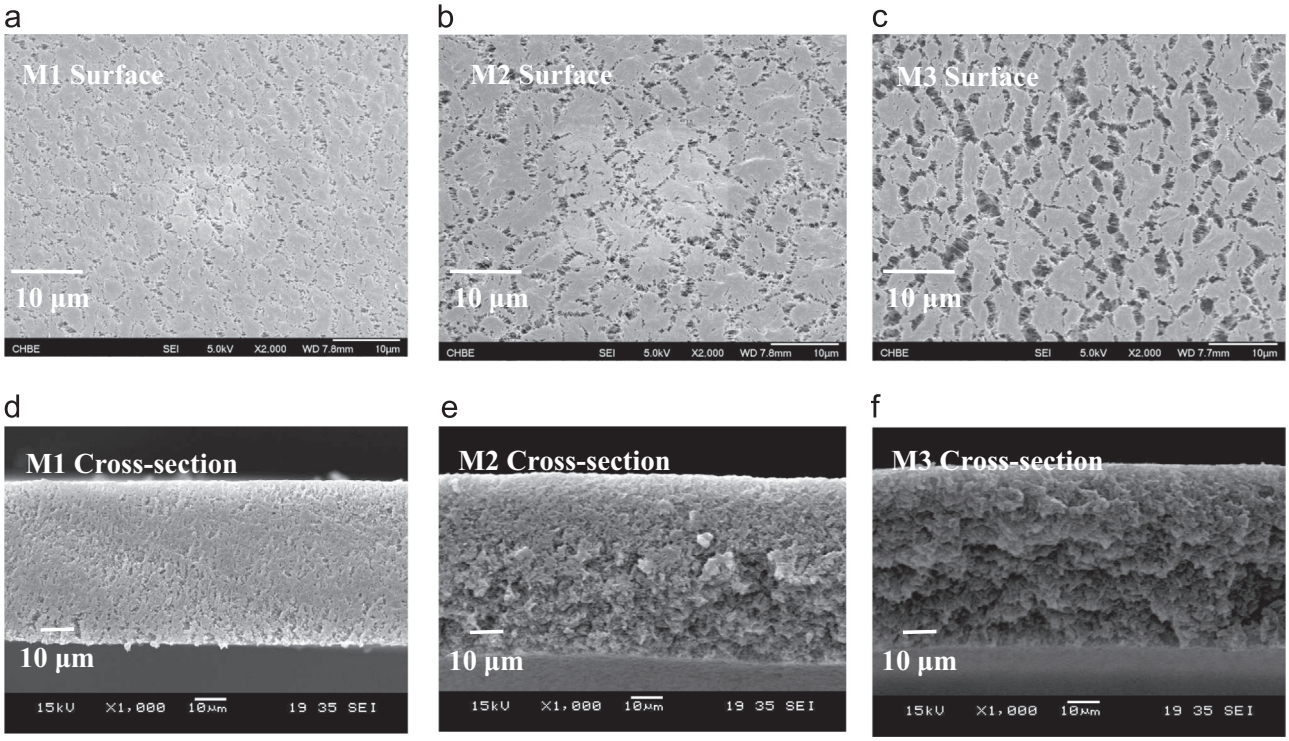

Fig. 3. Surface and cross-section morphology of PE membranes M1, M2 and M3.

Table 1
The specifications of the PE flat sheet membranes.

Membrane	M1	M2	M3	M4
Commercial name	TPZP	TPVG	TPGP	UPZP
Pore Size provided (μm)	0.05	0.10	0.20	0.05
Pore size measured (μm)	0.06 ± 0.03	0.10 ± 0.04	0.21 ± 0.05	0.05 ± 0.02
Porosity (%)	56.5 ± 5.5	63.2 ± 6.1	66.1 ± 7.2	50.3 ± 5.0
Thickness (μm)	45.0 ± 3.2	47.6 ± 3.0	50.4 ± 2.4	65.0 ± 3.8
Contact angle (°)	83.2 ± 2	106.4 ± 2	108.3 ± 3	85.3 ± 3
LEP (bar)	0.5 ± 0.05	0.6 ± 0.05	0.7 ± 0.05	0.7 ± 0.05

Fig. 3(d–f) exhibits the cross-sections morphology of the three PE membranes. It can be seen that the cross-sections are comprised of sponge-like structures. Compared to macrovoid structures, sponge-like structures possess several advantages. Firstly, it helps to increase membrane wetting resistance owing to the higher tortuosity and narrower pore size distribution [25,28]. In addition, sponge-like structures may provide better performance stability, especially in long term runs [10,29]. Despite of the macrovoid-free structures, the membranes still maintain relatively large porosities. As tabulated in Table 1, the highest porosity reaches to 66.1%. Generally, membranes with a high porosity and a lower thermal conductivity are desirable to maximize the water vapor mass transfer while minimize the heat loss from feed side to the permeate side during the DCMD process. The porosities show an increasing trend for the three membranes M1 to M3. The effect of porosity on membrane performance will be further tested. These morphologies are expected to provide effective water vapor permeation pathways while not sacrificing membrane wetting resistance.

Table 1 summarizes the thicknesses of PE membranes, which are around 50 μm and comparable for all 3 samples. In this study, the effects of membrane thickness on MD performance and energy efficiency are further investigated. Another PE membrane M4 with a similar pore size as M1 but a different thickness of 65 μm is also utilized. The detailed results and comparison will be discussed later.

3.1.2. Membrane hydrophobicity and LEP

Membrane hydrophobicity is one of the essential requirements to prevent membrane wetting. Table 1 presents the water contact angles of membranes M1, M2 and M3. All the three membranes show hydrophobic surfaces. However, M1 has the smallest contact angle, while M3 has the largest. This difference may be caused by the change in surface roughness. It has been reported that an increase in surface roughness can lead to an increase in membrane contact angle [30]. Table 2 lists their surface roughness characterized by AFM. The three roughness values; namely, root mean square roughness (R_{ms}), average roughness (R_a) and maximum roughness (R_{max}) all follow an increasing order from M1 to M3. This aligns exactly with the order of water contact angle, which supports the above proposition. The membrane surface contact angle would affect membrane wetting properties, LEP and permeation fluxes. As studied in Dumee et al.'s work [31], a lower surface contact angle favors the initial wetting of membranes. This will lead to the formation of a thin layer of liquid at membrane surface, which reduces the permeation flux of MD [31,32]. On the other hand, a higher contact angle may contribute to a better vapor transport. This is possibly because of the existence of a thin air film on membrane surfaces created by the hydrophobic forces. This film may effectively reduce the temperature polarization effect and enhance the evaporation of water at the boundary layer. Therefore, a higher contact angle would increase the MD

Table 2
Surface roughness of the three PE membranes M1, M2 and M3.

Membranes	Pore size (μm)	R_{ms} (nm)	R_a (nm)	R_{max} (nm)
M1	0.06	47.5	34.3	335.7
M2	0.10	67.6	54.5	383.1
M3	0.21	75.8	62.2	481.2

Root mean square roughness (R_{ms}), average roughness (R_a) and maximum roughness (R_{max}).

permeation flux.

LEP is a quantitative indication of membrane wetting resistance. As shown in Table 1, the measured LEP values for M1, M2 and M3 are 0.5, 0.6 and 0.7 bar, respectively. These values are all larger than the typical DCMD operation pressure of 0.1–0.3 bar. Since LEP is defined as the minimum pressure for a trace amount of liquid permeating through the membrane, these data imply that the PE membranes could prevent the penetration of feed solutions. In other words, these membranes are suitable for DCMD. It is worth noting that the LEP value has an increasing trend from M1 to M3, which follows the same order of membrane hydrophobicity. This confirms the importance of membrane hydrophobicity. Nonetheless, it is also noted that the LEP values for current PE membranes are not as high as some other MD membranes in the literature. This might be due to the relatively large surface pore sizes. As calculated from the AFM measurements, the average surface pore size values of M1 to M3 membranes are 0.5, 1.1 and 1.8 μm, respectively. These results could justify the relatively low LEP values obtained. To validate whether these LEP would limit the membrane long term performance, a 100 h MD experiment is carried out. The result will be discussed later.

3.2. Effects of operation parameters on PE membrane performance and energy efficiency

3.2.1. Effect of feed flow rate

Fig. 4(a) shows the MD permeation flux as a function of feed flow rate for membrane M1 at a feed temperature of 60 °C. The results reflect that the feed flow rate has a significant influence on membrane permeation flux. With the feed flow rate increased from 30 to 90 L/h, the permeation flux increases 85%. Such observation could be explained by the reduced temperature polarization effect [33–35]. To support this, the Reynolds numbers at the three flow rates are calculated according to the following equation:

$$Re = \frac{\rho v D}{\mu} \tag{5}$$

where Re is the Reynolds number, ρ is the density of fluid, v is the linear velocity of fluid, D is the diameter of the flow pipe and μ is the dynamic viscosity of fluid. The linear velocities correspond to the volumetric velocities 30, 60 and 90 L/h are calculated to be 0.08, 0.17 and 0.25 m/s, respectively. For rectangular flow channels, the diameter D is defined as in Eq. (6):

$$D = 4A/P \tag{6}$$

where A is the cross-section area and P is the perimeter. Therefore, the obtained Reynolds numbers at the three flow rates are 936, 1872 and 2809, respectively. Thus, at a higher feed flow rate, the Reynolds number increases. Thus, a better mixing is achieved between the bulk solution and the solution at membrane surface. This effectively increases the heat transfer coefficient and decreases the thermal boundary layer thickness, and hence reduces the temperature polarization. As the heat transfer becomes more efficient at the membrane surface, the membrane surface temperature at the feed side goes up which leads to mass transfer driving force increase and hence a higher permeation flux. In addition, a higher feed flow rate minimizes the temperature drop along the membrane surface. This would maintain the driving force over the entire membrane module and lead to a higher permeation flux [36]. Since a higher feed flow rate is more desirable, a flow rate of 90 L/h is therefore chosen in all subsequent studies.

3.2.2. Effect of feed temperature

Fig. 4(b) plots the permeation flux versus feed solution temperature for membrane M1 at a constant feed flow rate of 90 L/h. The curve displays an exponential increase of permeation flux with increasing feed temperature. This is owing to the exponential dependency of water vapor pressure with temperature as predicted by Antoine equation [37]. At the feed temperature of 80 °C, a high permeation flux of 83.3 L/m^2 h is achieved from the PE membrane, which demonstrates the potential of these commercial PE membranes to achieve high MD fluxes.

To understand the stability of this PE membrane at various feed temperatures, a DSC measurement was conducted. Fig. 5 shows the thermal response curve of the PE membrane sample. The polymer exhibits an endothermic transition characteristics and the melting point is 136 °C. This temperature is well above the DCMD operation temperatures, and assures the feed temperatures do not affect the PE membrane.

The effect of feed temperature on energy efficiency is also analyzed. Coupled with mass transport across the membrane, heat is also transferred through two aspects: (1) the vaporization and condensation heat of the permeating molecules, and (2) the conduction heat across the membrane. The formal heat is the effective heat, while the latter is usually denoted as an undesirable heat loss. Therefore, the membrane energy efficiency is defined as the ratio of the useful latent heat to the total heat that is transferred across the membrane [38]. The following equation can be used to calculate the energy efficiency (EE):

$$\mathrm{EE} = \frac{N_w \Delta H_v A}{N_w \Delta H_v A + h_m (T_f - T_p) A} = \frac{N_w \Delta H_v A}{m_p c_{pspec} (T_{pout} - T_{pin})} \tag{7}$$

where N_w is the permeation flux, ΔH_v is the latent heat of water evaporation, A is the membrane area, h_m is the membrane heat transfer coefficient, T_f and T_p are the average temperatures of the feed and permeate sides, m_p is the mass flow rate of the permeate stream, c_{pspec} refers to the average specific heat capacity of the permeate solution, T_{pout} and T_{pin} are the outlet and inlet

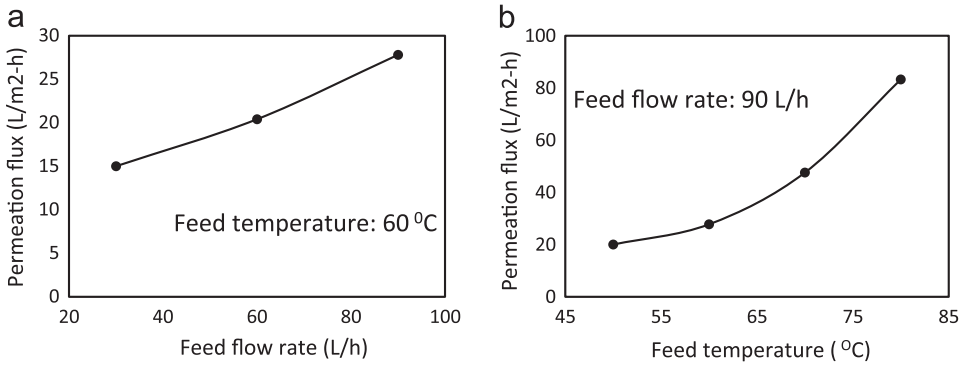

Fig. 4. DCMD permeation flux as a function of: (a) feed flow rate and (b) feed temperature for membrane M1.

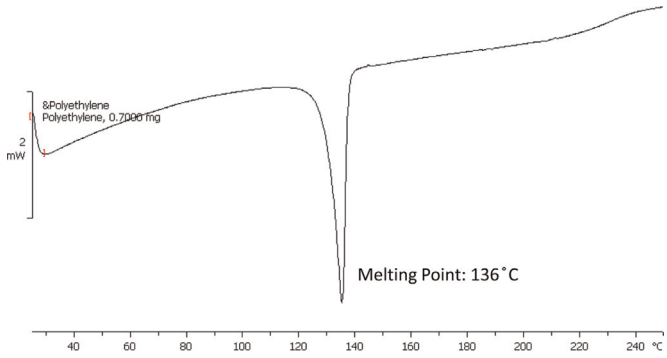

Fig. 5. The DSC thermogram of the PE membrane sample M1.

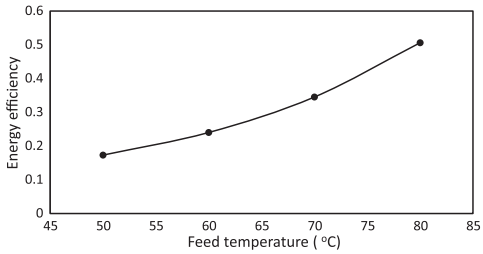

Fig. 6. Calculated energy efficiency versus feed solution temperature for membrane M1. Feed flow rate: 90 L/h.

temperatures of the permeate solution at the membrane module, respectively.

As depicted in Fig. 6, the energy efficiency increases with increasing feed temperature. This is because the driving force for mass transfer increases exponentially with feed temperature, while the conducting heat loss through the membrane increases linearly. Therefore, at a higher temperature, the numerator in Eq. (7) increases much faster than the de-numerator, and thus the energy efficiency increases. The overall energy efficiency obtained for the current PE membrane may be relatively low compared to some PP or PVDF membranes [11,39]. This is probably due to its higher thermal conductivity. Although the PE material has a low thermal conductivity of 0.40 W/m K, it is still much higher than those of PP (0.17 W/m K) and PVDF (0.19 W/m K) materials [20]. This would lead to a higher conductive heat loss across the membrane. Therefore, the thermal efficiency of PE membranes is lower than those of PP and PVDF membranes.

3.3. Effect of PE membranes properties on DCMD performance and energy efficiency

3.3.1. Effect of membrane pore size and porosity

To assess the potential of PE membranes, the effects of pore size and porosity on membrane performance are investigated. Fig. 7 shows the MD permeation fluxes for membranes M1, M2 and M3. Under the same operation conditions, M3 has the highest flux while M1 shows the lowest. This is explainable because their pore sizes and porosity follow the trend M3 > M2 > M1. A larger pore size and porosity may contribute to the DCMD performance through two mechanisms: (1) the direct effect is from the reduction of mass transfer resistance and (2) the indirect mechanism is from the decrease in thermal conductivity across the membrane because the air-filled pores in the membrane has a much lower conductivity than the polymer material. Thus, the undesirable heat loss is minimized and the driving force for vaporization is enhanced. Fig. 8 compares the energy efficiency of the three membranes and indicates the energy efficiency increasing from M1 to M3 under the same operation conditions. This further confirms the

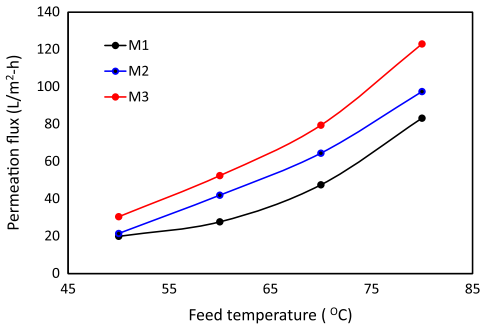

Fig. 7. DCMD permeation flux as a function of feed temperature at a feed flow rate of 90 L/h for membrane M1, M2 and M3.

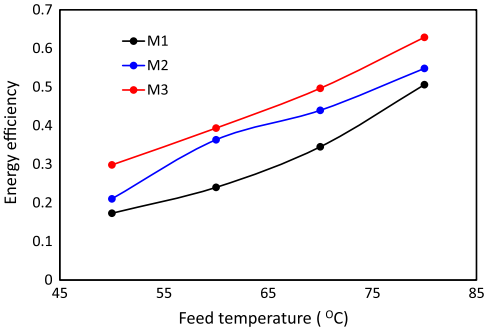

Fig. 8. Calculated energy efficiency versus feed solution temperature for membrane M1, M2 and M3.

proposition that a higher porosity membrane reduces the thermal conductivity and increases the energy efficiency.

Table 3 shows a comparison of DCMD performance between literature data and this work in almost the same temperature range [10,17,25,40–46]. The PE membranes exhibit a permeation flux surpassing most of the prior commercial and lab-made flat sheet and hollow fiber membranes. The best one is from M3 which reaches 123.0 L/m^2 h at 80 °C feed temperature. It might be noticed that current PE membranes may have a relatively smaller porosity compared to some PP or PVDF membranes. However, other than porosity, pore structures and pore interconnectivity also play important roles in determining membrane flux. Ideally, inter-connected open-cell pore structure can effectively form vapor transport channels. On the other hand, if the pores are not connected or closed, the mass transport resistance might be largely increased [11]. Therefore, despite of a possibly lower porosity of current PE membranes, their open pore structures may still contribute to the high permeation flux. The results obviously prove the capability of these PE membranes in MD applications.

3.3.2. Effect of membrane thickness

Membrane thickness is another important variable that affects the mass and heat transfer in MD [47]. Generally, a higher membrane thickness would lead to a larger mass transfer resistance and lower permeation flux. The relationship between membrane flux and thickness may be written as follow [47]:

$$N_w \propto \frac{r^{\alpha}\varepsilon}{\delta_m \tau} \tag{8}$$

where r is the mean pore size of membrane, the superscription α is a constant factor, ε is the membrane porosity, δ_m is the membrane thickness and τ is the membrane tortuosity. As such, to obtain a high permeation flux, the membrane thickness should be as thin as possible. On the contrary, a thicker membrane is beneficial to reduce the conductive heat loss across the membrane, which

Table 3
A comparison of DCMD performance for desalination.

Membrane	Feed inlet temp. (°C)	Feed NaCl conc. (wt%)	Feed flow rate (m/s)	Permeate inlet temp. (°C)	Membrane thickness (μm)	Flux (L/m^2-h)	Reference
Flat sheet membranes:							
CF_4 modified PES flat sheet	74.5	4.0	0.4	20	201	40.9	[41]
PVDF/nonwoven flat sheet	80.5	3.5	0.3	20	67	47.6	[42]
Commercial PTFE flat sheet	80	3.5	–	20	–	35.0	[43]
Commercial PTFE flat sheet	80	1.3	–	20	100	88.8	[44]
Commercial PP flat sheet	80	1.3	–	20	160	71.0	[44]
Hollow fiber membranes:							
CF_4 modified PES hollow fiber	73.8	4.0	2.0	20	236	66.7	[41]
PVDF multi-bore hollow fiber	80	3.5	0.4	17	50	48.0	[17]
PVDF single-layer hollow fiber	79.5	3.5	1.9	17.5	127	46.1	[10]
PVDF single-layer hollow fiber	81.3	3.5	1.8	17.5	190	79.2	[25]
PVDF dual-layer hollow fiber	80.4	3.5	1.8	15.3	50	66.9	[45]
PVDF dual-layer hollow fiber	80	3.5	1.4	17	153	83.4	[40]
Commercial PP hollow fiber	90	1.0	2.3	17	150	79.0	[46]
Commercial PE membrane M1	80	3.5	0.2	17	45	83.3	This work
Commercial PE membrane M2	80	3.5	0.2	17	48	97.5	This work
Commercial PE membrane M3	80	3.5	0.2	17	50	123.0	This work

increases the trans-membrane flux [48,49]. Thus, a balance between mass and heat transfer should be attained by designing an appropriate membrane thickness.

Fig. 9(a) and (b) exhibits the permeation flux and energy efficiency of the two PE membranes M1 and M4, where M4 has a similar pore size as M1 but a higher thickness. The results show that when the membrane thickness is higher, the permeation flux is lower. This is reasonable because of the inversely proportional relationship between membrane thickness and flux. Moreover, the energy efficiency of M4 is also slightly lower than that of M1. This may be attributed to two effects: (1) according to Eq. (4), the energy efficiency depends on the ratio of heat convected by evaporation to heat loss by conduction. The evaporative heat transfer is associated with membrane flux, and is inversely proportional to membrane thickness. The relationship between conductive heat loss and membrane thickness could be expressed by Fourier's law:

$$h_m \propto \frac{k}{\delta_m} \tag{9}$$

where h_m is the membrane heat transfer coefficient, k is membrane thermal conductivity and δ_m is the membrane thickness. The k value depends on membrane material as well as membrane porosity and pore size. To isolate the effect of membrane porosity, it is firstly assumed to be the same for both M1 and M4. In addition, since both M1 and M4 are made of the PE material and have a similar pore size, the thermal conductivity term is then a constant for both membranes. By substituting the convective and conductive heat transfer terms in Eq. (7) with Eqs. (8) and (9), the energy efficiency may be written as:

$$EE \propto \frac{\frac{1}{\delta_m}\Delta H_v A}{\frac{1}{\delta_m}\Delta H_v A + \frac{1}{\delta_m}(T_f - T_p)A} = \frac{\Delta H_v A}{\Delta H_v A + (T_f - T_p)A} \tag{10}$$

Therefore, the thickness term is canceled in the EE equation. However, when both the evaporative heat transfer and heat loss are reduced at a higher membrane thickness, the average feed and permeate side temperatures T_f and T_p tend to approach their inlet temperatures, respectively. Thus, the difference $T_f - T_p$ becomes larger, which means the denominator in Eq. (7) becomes larger. Consequently, the energy efficiency decreases when membrane thickness is increased. Nonetheless, it is worth noting that the degrees of feed and permeate side temperature changes are not large, especially at lower feed temperatures. There is only a small window that one may observe energy efficiency change. Therefore, in Fig. 9(b), the effect of membrane thickness only reveals at higher operation temperatures.

(2) The other reason that may result in a lower energy efficiency of M4 is its lower porosity. As discussed in Section 3.3.1, a less porous membrane has a higher thermal conductivity, which results in a higher heat loss. To validate the hypothesis, the porosity of M4 is measured to be 50.3%. This value is smaller than that (56.5%) of M1, and confirms the above suggestion. As a result, M1 is a better choice for MD owing to have the good balance between thickness and porosity.

3.4. Long term performance of the PE membrane

Through the investigation of short term membrane

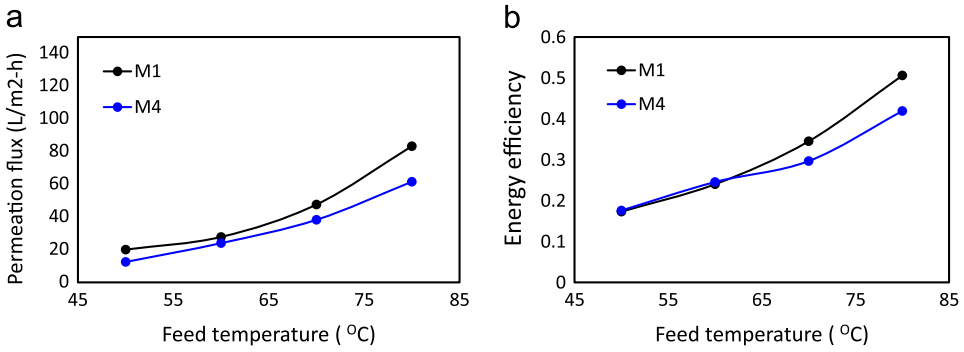

Fig. 9. (a) MD permeation flux and (b) energy efficiency for membrane M1 and M4 at a feed flow rate of 90 L/h.

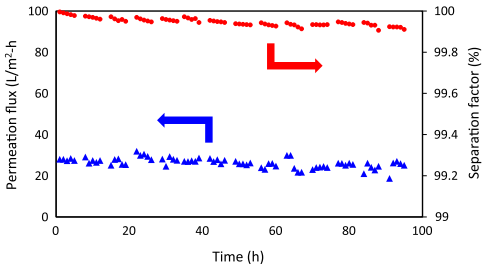

Fig. 10. Permeation flux and separation factor of M1 under a 100-h operation.

performance, exceptional MD separation performance have been discovered for these PE membranes. Therefore, a long term DCMD experiment was conducted on membrane M1 for a period of 100 h. The resultant permeation flux and separation factor are plotted in Fig. 10. A relatively stable performance is observed during the entire experiment. The relatively stable performance is attributed by the hydrophobic nature of the PE membrane. Therefore, the surface wetting is not severe during the initial part of the testing. However, since the PE membrane has a large surface pore size, partial pore wetting may occur after sometime. This might lead to the formation of a thin layer of liquid at membrane surface, which reduces mass and heat transfer rate at the boundary [31,32]. Hence, a slight decline of permeation flux is noticed after 60-h running probably due to partial membrane pore wetting [50]. Besides, the separation factor is maintained higher than 99.9% throughout the test, although a minor reduction is observed with increasing operation time because of the partial wetting [40]. Nonetheless, the relatively stable performance signifies the feasibility of using these PE membranes for MD application.

4. Conclusions

In this work, several commercial PE membranes have been employed in DCMD for seawater desalination. The feasibility and separation performance of using these PE membranes for this application have been demonstrated. In-depth investigations on the effects of membrane physicochemical properties and MD operation parameters on permeation flux and energy efficiency were investigated. The following conclusions can be drawn from the current study:

(1) These PE membranes are intrinsically hydrophobic with good stability in seawater and low thermal conductivity. Their sponge-like morphology, appropriate pore size, porosity, thickness and reasonable wetting resistance make these PE membranes good candidates for MD application.
(2) The effects of feed solution flow rate and temperature on membrane performance were investigated. A higher feed flow rate leads to a higher permeation flux, owing to the reduced temperature polarization effect. With an increase in feed temperature, both MD permeation flux and energy efficiency increase because of the exponential increase in driving force for mass transfer of water vapor with feed temperature.
(3) The PE membrane with larger pore size and porosity shows better MD performance in terms of flux and energy efficiency. This is attributed to the increased mass transfer rate and reduced thermal conductivity. The best permeation flux from M3 reaches 123.0 L/m^2 h at 80° C feed temperature. The superior performance surpasses most of the prior commercial and lab-made flat sheet and hollow fiber membranes.
(4) Through the long term MD testing of 100 h, a relatively stable performance is observed during the entire experiment. This long term stability signifies the feasibility of using these PE membranes for MD application.

Acknowledgment

This research was funded by the Singapore National Research Foundation under its Competitive Research Program for the project entitled, “Advanced FO Membranes and Membrane Systems for Wastewater Treatment, Water Reuse and Seawater Desalination” (Grant number: R-279-000-336-281). The authors also thank the Singapore National Research Foundation under its Energy Innovation Research Programme for the project entitled, “Using Cold Energy from Re-gasification of Liquefied Natural Gas (LNG) for Novel Hybrid Seawater Desalination Technologies” (Grant number: R-279-000-456-279) for funding this research. We would also gratefully thank Entegris Inc. for proving the PE membranes and their support. Dr. Zuo Jian also acknowledges the World Future Foundation for his Ph.D. Prize in Environmental ans Sustainability Research 2015.

Nomenclature

Abbreviations

AFM	atomic force microscope
AGMD	air gas membrane distillation
DCMD	direct contact membrane distillation
DSC	differential scanning calorimeter
EE	energy efficiency
FESEM	field emission scanning electron microscopy
LEP	liquid entry pressure
MD	membrane distillation
MED	multiple-effect distillation
MSF	multi-stage flash distillation
NaCl	sodium chloride
PE	polyethylene
PES	polyethersulfone
PP	polypropylene
PTFE	polytetrafluoro-ethylene
PVDF	polyvinylidene fluoride
SGMD	sweep gas membrane distillation
SWRO	sea water reverse osmosis
VMD	vacuum membrane distillation

Symbols

A	membrane area
c_f	NaCl concentration in feed solution
c_p	NaCl concentration in permeate solution
c_{pspec}	specific heat capacity
h_m	membrane heat transfer coefficient
ΔH_v	latent heat of water evaporation
m	mass of the permeate sample
m_{memb}	weight of a piece of membrane
m_p	mass flow rate of the permeate stream
N_w	permeation flux
t	time
T_f	the average temperatures of the feed side
T_p	the average temperatures of the permeate side
T_{pin}	inlet temperature of the permeate solution
T_{pout}	outlet temperature of the permeate solution
V_{memb}	volume of a piece of membrane

r	the mean pore size of membrane
R_a	average roughness
R_{max}	maximum roughness
R_{ms}	root mean square roughness
ρ_{mater}	density of the membrane material
ε	porosity
α	constant factor
β	separation factor
δ_m	membrane thickness
τ	membrane tortuosity

References

[1] Water scarcity, International decades for action "Water for Life" 2005–2015. Retrieved from ⟨http://www.un.org/waterforlifedecade/scarcity.shtml⟩, 25 March 2015.
[2] R.F. Service, Desalination freshens up, Science 313 (2006) 1088–1090.
[3] I.C. Escobar, A summary of challenges still facing desalination and water reuse, in: I.C. Escobar, A.L. Schafer (Eds.), Sustainable Water for the Future – Water Recycling Versus Desalination, Elsevier Science, The Netherlands, 2007, pp. 389–397.
[4] K.W. Lawson, D.R. Lloyd, Membrane distillation (review), J. Membr. Sci. 124 (1997) 1–25.
[5] L. Song, Z. Ma, X. Liao, P.B. Kosaraju, J.R. Irish, K.K. Sirkar, Pilot plant studies of novel membranes and devices for direct membrane distillation-based desalination, J. Membr. Sci. 323 (2008) 257–270.
[6] E. Curcio, E. Drioli, Membrane distillation and related operations – a review, Sep. Purif. Rev. 34 (2005) 35–86.
[7] M. Khayet, Membranes and theoretical modeling of membrane distillation: a review, Adv. Colloid Interface Sci. 164 (2011) 56–88.
[8] M. Gryta, Water purification by membrane distillation process, Sep. Sci. Technol. 41 (2006) 1789–1798.
[9] B.R. Bodell, Silicone Rubber Vapor Diffusion in Saline Water Distillation, US patents 285032, 1963.
[10] M.M. Teoh, T.S. Chung, Membrane distillation with hydrophobic macrovoid-free PVDF-PTFE hollow fiber membranes, Sep. Purif. Technol. 66 (2009) 229–236.
[11] P. Wang, M.M. Teoh, T.S. Chung, Morphological architecture of dual-layer hollow fiber for membrane distillation with higher desalination performance, Water Res. 45 (2011) 5489–5500.
[12] D. Singh, K.K. Sirkar, Desalination of brine and produced water by direct contact membrane distillation at high temperatures and pressure, J. Membr. Sci. 389 (2012) 380–388.
[13] M. Tomaszewska, Membrane distillation, Environ. Prot. Eng. 25 (1999) 37–47.
[14] M. Khayet, T. Matsuura, Preparation and characterization of polyvinylidene fluoride membranes for membrane distillation, Ind. Eng. Chem. Res. 40 (2001) 5710–5718.
[15] M. Gryta, M. Tomaszewska, J. Grzechulska, A.W. Morawski, Membrane distillation of NaCl solution containing natural organic matter, J. Membr. Sci. 181 (2001) 279–287.
[16] H. Maab, I. Francis, A. Al-saadi, C. Aubry, N. Ghaffour, G. Amy, S.P. Nunes, Synthesis and fabrication of nanostructured hydrophobic polyazole membranes for low-energy water recovery, J. Membr. Sci. 423–424 (2012) 11–19.
[17] P. Wang, T.S. Chung, Design and fabrication of lotus-root-like multi-bore hollow fiber membrane for direct contact membrane distillation, J. Membr. Sci. 421–422 (2012) 361–374.
[18] L.T. Huang, P.S. Hsu, C.Y. Kuo, S.C. Chen, J.Y. Lai, Pore size control of PTFE membranes by stretch operation with asymmetric heating system, Desalination 233 (2008) 64–72.
[19] C. Chandavasu, M. Xanthos, K.K. Sirkar, C.G. Gogos, Fabrication of microporous polymeric membranes by melt processing of immiscible blends, J. Membr. Sci. 211 (2003) 167–175.
[20] P. Wang, T.S. Chung, Recent advances in membrane distillation processes: membrane development, configuration design and application exploring, J. Membr. Sci. 474 (2015) 39–56.
[21] J.G. Lee, Y.D. Kim, W.S. Kim, L. Francis, G. Amy, N. Ghaffour, Performance modeling of direct contact membrane distillation (DCMD) seawater desalination process using a commercial composite membrane, J. Membr. Sci. 478 (2015) 85–95.
[22] M. Gryta, Influence of polypropylene membrane surface porosity on the performance of membrane distillation process, J. Membr. Sci. 287 (2007) 67–78.
[23] J.M. Li, Z.K. Xu, Z.M. Liu, W.F. Yuan, H. Xiang, S.Y. Wang, Y.Y. Xu, Microporous polypropylene and polyethylene hollow fiber membranes, Part 3. Experimental studies on membrane distillation for desalination, Desalination 155 (2003) 153–156.
[24] S. Bonyadi, T.S. Chung, Flux enhancement in membrane distillation by fabrication of dual layer hydrophilic–hydrophobic hollow fiber membranes, J. Membr. Sci. 306 (2007) 134–146.
[25] K.Y. Wang, S.W. Foo, T.S. Chung, Mixed matrix PVDF hollow fiber membranes with nanoscale pores for desalination through direct contact membrane distillation, Ind. Eng. Chem. Res. 48 (2009) 4474–4483.
[26] M.S. El-Bourawi, Z. Ding, R. Ma, M. Khayet, A framework for better understanding membrane distillation separation process, J. Membr. Sci. 285 (2006) 4–29.
[27] E. Drioli, Y. Wu, V. Calabro, Membrane distillation in the treatment of aqueous solutions, J. Membr. Sci. 33 (1987) 277–284.
[28] M.C. Garcia-Payo, M.A. Izquierdo-Gil, C. Fernandez-Pineda, Wetting study of hydrophobic membranes via liquid entry pressure measurements with aqueous alcohol solutions, J. Colloid Interface Sci. 230 (2) (2000) 420–431.
[29] N. Widjojo, T.S. Chung, M. Weber, C. Maletzko, V. Warzelhan, The role of sulphonated polymer and macrovoid-free structure in the support layer for thin-film composite (TFC) forward osmosis (FO) membranes, J. Membr. Sci. 383 (2011) 214–223.
[30] C.Y. Kuo, H.N. Lin, H.A. Tsai, D.M. Wang, J.Y. Lai, Fabrication of a high hydrophobic PVDF membrane via nonsolvent induced phase separation, Desalination 233 (2008) 40–47.
[31] L.F. Dumee, S. Gray, M. Duke, K. Sears, J. Schutz, N. Finn, The role of membrane surface energy on direct contact membrane distillation performance, Desalination 323 (2013) 22–30.
[32] H. Asanuma, H. Noguchi, K. Uosaki, H.Z. Yu, Water structure at superhydrophobic quartz/water interfaces: a vibrational sum frequency generation spectroscopy study, J. Phys. Chem. C 113 (2009) 21155–21161.
[33] Y.D. Kim, K. Thu, N. Ghaffour, K.C. Ng, Performance investigation of a solar assisted direct contact membrane distillation system, J. Membr. Sci. 427 (2013) 345–364.
[34] H.J. Hwanga, K. He, S. Gray, J. Zhang, I.S. Moon, Direct contact membrane distillation (DCMD): experimental study on the commercial PTFE membrane and modelling, J. Membr. Sci. 371 (2011) 90–98.
[35] M.M. Teoh, N. Peng, T.S. Chung, L.L. Koo, Development of novel multi-channel rectangular membranes with grooved outer selective surface for membrane distillation, Ind. Eng. Chem. Res. 50 (24) (2011) 14046–14054.
[36] L. Song, B. Li, K.K. Sirkar, J.L. Gilron, Direct contact membrane distillation-based desalination: novel membranes, devices, larger-scale studies and a model, Ind. Eng. Chem. Res. 46 (2007) 2307.
[37] S. Bonyadi, T.S. Chung, Highly porous and macrovoid-free PVDF hollow fiber membranes for membrane distillation by a solvent-dope solution co-extrusion approach, J. Membr. Sci. 331 (2009) 66–74.
[38] K. Smolders, A.C.M. Franken, Terminology for membrane distillation, Desalination 72 (3) (1989) 249–262.
[39] M. Gryta, Effectiveness of water desalination by membrane distillation process, Membrane 2 (2012) 415–429.
[40] F. Edwie, M.M. Teoh, T.S. Chung, Effects of additives on dual-layer hydrophobic–hydrophilic PVDF hollow fiber membranes for membrane distillation and continuous performance, Chem. Eng. Sci. 68 (2012) 567–578.
[41] X. Wei, B. Zhao, X.M. Li, Z. Wang, B.Q. He, T. He, B. Jiang, CF_4 plasma surface modification of asymmetric hydrophilic polyethersulfone membranes for direct contact membrane distillation, J. Membr. Sci 407–408 (2012) 164–175.
[42] D. Hou, G. Dai, J. Wang, H. Fan, L. Zhang, Z. Luan, Preparation and characterization of PVDF/nonwoven fabric flat-sheet composite membranes for desalination through direct contact membrane distillation, Sep. Purif. Technol. 101 (2012) 1–10.
[43] M.M.A. Shirazi, A. Kargari, M. Tabatabaei, Evaluation of commercial PTFE membranes in desalination by direct contact membrane distillation, Chem. Eng. Process. 76 (2014) 16–25.
[44] L. Francis, N. Ghaffour, A.S. Alsaadi, S.P. Nunes, G.L. Amy, Performance evaluation of the DCMD desalination process under bench scale and large scale module operating conditions, J. Membr. Sci. 455 (2014) 103–112.
[45] M. Su, M.M. Teoh, K.Y. Wang, J. Su, T.S. Chung, Effect of inner-layer thermal conductivity on flux enhancement of dual-layer hollow fiber membranes in direct contact membrane distillation, J. Membr. Sci. 364 (2010) 278–289.
[46] B.A. Li, K.K. Sirkar, Novel membrane and device for direct contact membrane distillation-based desalination process, Ind. Eng. Chem. Res. 43 (2004) 5300–5309.
[47] S. Simone, A. Figoli, A. Criscuoli, M.C. Carnevale, A. Rosselli, E. Drioli, Preparation of hollow fibre membranes from PVDF/PVP blends and their application in VMD, J. Mater. Sci. 364 (2010) 219–232.
[48] M. Khayet, M.P. Godino, J.I. Mengual, Possibility of nuclear desalination through various membranes distillation configurations: a comparative study, Int. J. Nucl. Desalination 1 (1) (2003) 30–46.
[49] R.W. Schofield, A.G. Fane, C.J.D. Fell, Heat and mass transfer in membrane distillation, J. Membr. Sci. 33 (1987) 299–313.
[50] M. Gryta, M. Barancewicz, Influence of morphology of PVDF capillary membranes on the performance of direct contact membrane distillation, J. Membr. Sci. 358 (1–2) (2010) 158–167.